Composition controlled spin polarization in $Co_{1-x}Fe_xS_2$: Electronic, magnetic, and thermodynamic properties

L. Wang,[1] T. Y. Chen,[2] C. L. Chien,[2] J. G. Checkelsky,[3] J. C. Eckert,[3] E. D. Dahlberg,[4] K. Umemoto,[1,5] R. M. Wentzcovitch,[1,5] and C. Leighton[1,*]

[1]*Department of Chemical Engineering and Materials Science, University of Minnesota, 151 Amundson Hall, 421 Washington Avenue SE, Minneapolis, Minnesota 55455, USA*

[2]*Department of Physics and Astronomy, The Johns Hopkins University, 3400 North Charles Street, Baltimore, Maryland 21218, USA*

[3]*Department of Physics, Harvey Mudd College, 301 E. 12th Street, Claremont, California 91711, USA*

[4]*School of Physics and Astronomy, University of Minnesota, 116 Church Street SE, Minneapolis, Minnesota 55455, USA*

[5]*Supercomputer Institute, University of Minnesota, 117 Pleasant Street SE, Minneapolis, Minnesota 55455, USA*

(Received 3 January 2006; revised manuscript received 6 March 2006; published 3 April 2006)

We recently demonstrated that alloy composition can be used to fine tune the position of the Fermi level in $Co_{1-x}Fe_xS_2$ alloys leading to composition-controlled spin polarization and the ability to engineer high conduction electron spin polarizations of up to 85%. We present here a comprehensive experimental investigation of the structure, stoichiometry, magnetic, magnetotransport, and thermodynamic properties of bulk polycrystalline solid solutions of $Co_{1-x}Fe_xS_2$. These data are supplemented with direct measurements of the spin polarization at the Fermi level by point contact Andréev reflection (PCAR) and first principles electronic structure calculations. The compositions studied are in the range $0.0<x<0.30$, the most relevant part of the phase space in terms of composition control over high spin polarization. By measuring the Fe doping dependence of the saturation magnetization, high field magnetoresistance, and anisotropic magnetoresistance, and combining them with PCAR, we are able to show that Fe doping first leads to a crossover from minority to majority spin polarization, followed by attainment of a highly spin polarized state for $x>0.07$. The experimentally determined spin polarization can be tuned by alloy composition between -57% ($x=0$) and $+85\%$ ($x=0.15$). The evolution of the magnetic, transport, and thermodynamic properties with increasing Fe doping is discussed in terms of the composition dependence of the conduction electron spin polarization and the spin-dependent band structure.

DOI: 10.1103/PhysRevB.73.144402 PACS number(s): 75.47.-m, 72.25.Ba, 85.75.−d

I. INTRODUCTION

The emerging research field of spin-electronics, or spintronics, has received a great deal of attention in recent years.[1,2] As opposed to conventional microelectronics, where only the electronic charge carries information, both charge *and* spin are utilized in spintronics. This provides new routes for the design of novel devices that are faster, nonvolatile, and therefore have no boot-up time, and potentially have lower power consumption. In fact, first-generation spintronic devices are already in existence and are currently used, or are under development, in the magnetic recording industry. Examples include spin-valve and current perpendicular to the plane giant magnetoresistance read heads[1–4] and nonvolatile magnetic random access memory,[1,2,5] based on tunneling magnetoresistance.[1,2,6] Future generations of spintronic devices promise to combine technologically important nonmagnetic semiconductors with magnetism, either by synthesizing dilute magnetic semiconductors[1,2] or by fabricating heterostructures with conventional ferromagnetic metals.[1,2]

A key component common to all spintronic devices is a source of spin-polarized carriers, most commonly a ferromagnetic (FM) material. It is clear that in many cases the performance of the spintronic devices is dramatically improved if this electron source is highly polarized, i.e., if the polarization of the electron spins at the Fermi level (P) is large. In terms of the electronic band structure, spin polarization is usually defined by,[7]

$$P = \frac{N_\uparrow(E_F) - N_\downarrow(E_F)}{N_\uparrow(E_F) + N_\downarrow(E_F)}, \tag{1}$$

where $N_{\uparrow,\downarrow}(E_F)$ is the spin-dependent density of states (DOS) at the Fermi level E_F. Spin-polarized photoemission is a technique that is capable of providing such a direct measurement of P, but it suffers from poor energy resolution and extreme surface sensitivity.[8–10] Alternatively, the spin polarization can be probed by electron tunneling across an insulating barrier, either using two FM electrodes,[6] or one FM and one superconducting electrode (i.e., the Meservey-Tedrow method).[11] The tunneling spin polarization is defined by

$$P = \frac{N_\uparrow(E_F)|T_\uparrow|^2 - N_\downarrow(E_F)|T_\downarrow|^2}{N_\uparrow(E_F)|T_\uparrow|^2 + N_\downarrow(E_F)|T_\downarrow|^2}, \tag{2}$$

where $T_{\uparrow,\downarrow}$ is the (potentially spin-dependent) tunneling matrix element. Planar or point contact Andréev reflection (PCAR) can also be used to measure spin polarization,[12–20] the relevant definition being

$$P = \frac{N_\uparrow(E_F)v_{F,\uparrow} - N_\downarrow(E_F)v_{F,\downarrow}}{N_\uparrow(E_F)v_{F,\uparrow} + N_\downarrow(E_F)v_{F,\downarrow}}, \tag{3}$$

where v_F is the (potentially spin-dependent) Fermi velocity. If the electronic transport in the Andréev reflection measurement is diffusive, then v_F is replaced with v_F^2. It is therefore

important to note that different definitions of spin polarization are accessed in different experimental situations.[7]

Ferromagnets with $P=100\%$, also known as half-metallic ferromagnets (HMFs),[21] would be ideal materials for use as a source of polarized spins. Such materials have the Fermi level located in the conduction band for one spin orientation and in a gap for the opposite spin orientation, resulting in $P=100\%$. The advantages offered by these HMFs can be seen from the theoretical predictions,[22] and experimental observations,[23–25] of very large TMR in magnetic tunnel junctions as $P\rightarrow 100\%$, as well as the theoretical claims that efficient "Ohmic" spin injection[26,27] will only be possible in the limit $P\rightarrow 100\%$.[28]

The situation described above has led to an intensive search for HMFs. Indeed, several ferromagnets (or ferrimagents) have been the subject of experimental investigations concluding that the materials are either very highly polarized or completely half-metallic. CrO_2,[9,15,16,29] Fe_3O_4,[10,30] $La_{0.67}Sr_{0.33}MnO_3$[8,14,17,18] and $Ga_{0.95}Mn_{0.05}As$[31] are perhaps the most widely known examples, where P values have been found to lie in the range 80%–100% by various techniques. Of these, the strongest evidence, particularly from transport investigations,[15,29] occurs for CrO_2. It should be noted, however, that there still remain some controversies regarding the labeling of any of these compounds as "half-metallic,"[32] particularly at finite temperatures.[33,34] The fact that different definitions of P apply to different measurement modes (see above), and that spin polarizations derived from spin-resolved photoemission are sensitive to the wave vector and measurement conditions chosen,[32] both contribute to the difficulty in concluding true half-metallicity in these materials. There is a significant amount of theoretical work suggesting that excitations at finite temperatures lead to destruction of the fully polarized state even for systems that are half-metallic at $T=0$ (see Refs. 32–34), and there are several pieces of experimental evidence to support the notion that P is dramatically reduced at high temperatures.[8,32]

In addition to these general comments, several of these compounds suffer from key drawbacks such as metastability and incompatibility with conventional vacuum deposition techniques (CrO_2), poor conductivity at low temperatures (Fe_3O_4), low Curie temperature ($Ga_{1-x}Mn_xAs$), and rapid fall-off in polarization with increasing temperature ($La_{1-x}Sr_xMnO_3$, and CrO_2). It is therefore clear that it is very important for future progress that other highly polarized materials are developed. In addition, although it has not been discussed in the literature, FM systems with *tunable* spin polarization could be very useful for basic research in spintronics.[35] For instance, this would allow for the measurement of the device performance (e.g., TMR) as a function of the spin polarization of the FM electrodes, a feat that cannot be achieved with conventional transition metal ferromagnets. This is a desirable property even if the Curie temperatures of the materials in question are too low for technological applications; it would still allow for fundamental studies of spintronic devices as a function of the spin polarization. In this paper we demonstrate the application of a simple scheme that allows for composition control over the spin polarization of the ferromagnet $Co_{1-x}Fe_xS_2$.[35] We demonstrate the ability to deliberately engineer a highly polarized ferromagnet, as opposed to simply searching for one based on the results of electronic band structure predictions.

Our work is based on the pyrite structure itinerant ferromagnet CoS_2 (Curie temperature, $T_C=121$ K, electronic configuration $t_{2g}^6e_g^1$, $S=1/2$). Our recent determination of $P=57\%$ from PCAR confirms that the pure compound is *not* half-metallic.[36] The essential concept, which was alluded to by Zhao *et al.*[37] and put on a firm theoretical footing by Mazin,[38] exploits the fact that CoS_2 has a Fermi level that lies low in the conduction band[37–41] and that it can be alloyed with FeS_2, an isostructural diamagnetic semiconductor ($t_{2g}^6e_g^0$, $S=0$), with a reduced E_F.[37,38] The solid solution $Co_{1-x}Fe_xS_2$ is then expected to have an Fe concentration (x)-dependent Fermi level, implying that in a certain composition range E_F can be decreased such that it intersects the majority spin band while lying in a gap for the minority spins, producing $P=100\%$. (For a more detailed discussion, see our previous report[35].) Detailed band structure calculations have demonstrated that this simple concept of Fermi level manipulation by Fe doping is actually preserved; Mazin performed density functional theory calculations within the local spin density approximation on $Co_{1-x}Fe_xS_2$.[38] The linear muffin tin orbital (LMTO) method was used, and then checked with the full potential linear-augmented plane wave method. The results for the two methods agree very well and suggest that $Co_{1-x}Fe_xS_2$ is a HMF in the composition range $0.25<x<0.85$. Our band structure calculations[35] also show the spin polarization of $Co_{1-x}Fe_xS_2$ can be tuned by Fe doping, from -75% ($x=0.00$) to 100% ($x\geqslant 0.25$).[35] The sign change reflects a crossover from minority to majority spin dominance and is due to the specific shape of the density of states as a function of energy.[35]

The $Co_{1-x}Fe_xS_2$ system therefore offers substantial advantages over other candidate half-metals. First and foremost we are able to deliberately "engineer" high spin polarization by Fermi level control, as opposed to simply searching for half-metallic compounds based on the predictions of band structure calculations. Second, as pointed out by Mazin,[38] the high spin polarization in this system should not be sensitive to crystallographic disorder and defects, in contrast to other systems such as Heusler alloys.[19,20,42–44] Third, the composition control of the spin polarization offers unique opportunities for fundamental studies of material properties as a function of spin polarization, and finally, looking forward to heterostructure fabrication, this system has a close lattice match to important semiconductors such as Si and GaAs. It has even been suggested that interfaces between CoS_2 and such semiconductors are good candidates for efficient spin filtering.[45] Although the Curie temperatures are around 150 K, ruling out room temperature applications, it seems that the $Co_{1-x}Fe_xS_2$ alloy system offers great potential opportunities for the *fundamental* study of highly spin-polarized FMs and the heterostructured spintronic devices fabricated from them.

Despite considerable research efforts on the pyrite structure sulfides such as FeS_2 (as a possible candidate for photoelectrochemical and photovoltaic applications[46–49]), CoS_2 and NiS_2 (for their interesting magnetic and transport character[50–56]), $Co_{1-x}Fe_xS_2$ has received little attention.[35,36,41,50,52] We present here a brief review of the

previous work. Ogawa *et al.* investigated the saturation magnetization and Curie temperature of $Co_{1-x}Fe_xS_2$ for various Fe doping levels.[52] Their results show that the total saturation magnetization is proportional to cobalt concentration in the range $0.05<x<0.90$ and that the Curie temperature dependence on Fe doping shows a nonmonotonic behavior, attaining a maxium at $x=0.25$. Similar results were obtained by Jarrett *et al.*[57] Ogawa *et al.* also measured the zero magnetic field temperature dependence of the resistivity for $Co_{1-x}Fe_xS_2$.[50] Their results revealed an anomalous peak in the resistivity near T_C for low Fe doping, which is due to a band structure effect as discussed in a previous report of our own.[36] In the temperature range $T<T_C$, the transport characteristics of $Co_{1-x}Fe_xS_2$ change from metallic to semiconducting with increasing x, as expected (CoS_2 is a ferromagnetic metal, whereas FeS_2 is a diamagnetic semiconductor). More recently, PCAR measurements by Cheng *et al.* on $Co_{1-x}Fe_xS_2$ single crystals indicated spin-polarization values $<61\%$, far below the predicted 100%.[58] As discussed in detail later, these results differ from those presented here. We believe this is due to the nonstoichiometry explicitly noted by Cheng *et al.* (as discussed later). Ramesha *et al.* also recently reported magnetization measurements and band structure calculations on $Co_{1-x}Fe_xS_2$.[41] They presented magnetometry results on polycrystalline $Co_{1-x}Fe_xS_2$ synthesized at 400 °C. Their LMTO band structure calculation emphasized the importance of the antibonding S-S level for the half-metallic behavior of $Co_{1-x}Fe_xS_2$.

In this paper, we present a detailed investigation of the magnetic, electronic and thermodynamic properties of $Co_{1-x}Fe_xS_2$. We have studied ten compositions in the range $0.00<x<0.30$, in sulphur stoichiometric polycrystalline bulk materials. Our measurements indicate that the saturation magnetization per Co ion (M_S) increases with increasing doping level up to $x=0.07$, at which point it attains the ideal value of $1.0\mu_B$/Co ion, consistent with $P=100\%$. This integer value is maintained up to $x=0.30$. T_C versus doping level shows an intriguing nonmonotonic behavior with a maximum at $x=0.20$. The temperature dependence of the resisitivity (ρ) displays a hump near T_C for low doping, which evolves into a transition to a state with $d\rho/dT<0$ (i.e., a semiconducting-like temperature dependence) for $x>0.10$. A sizeable ($>10\%$ in 90 kOe) positive magnetoresistance (MR) is observed near T_C regardless of Fe doping level. These observations are consistently interpreted in terms of the spin dependent band structure of the $Co_{1-x}Fe_xS_2$ alloys. The negative MR below T_C, which is due to field suppression of electron-magnon scattering, vanishes at $x=0.07$, exactly coincident with the attainment of 1.0 μ_B/Co in the $M_S(x)$ measurement. We interpret this as a vanishing of the spin-flip electron-magnon scattering contribution to the resistivity, suggesting very high P at $x>0.07$. In addition, the anisotropic magnetoresistance (AMR) also shows a sign change from negative to positive with increasing doping level, the crossover occurring between $x=0.00$ and 0.03. This is interpreted, within the standard models of AMR, as being due to a sign change in P, consistent with our band structure calculations.[35] We also investigated the heat capacity (C_p) of $Co_{1-x}Fe_xS_2$. The DOS at E_F extracted from the low temperature $C_p(T)$ measurement decreases with increasing doping level, consistent with the behaviour of $\rho(T)$, and in reasonable quantitative agreement with theory. Finally, the PCAR measurements show 85% spin polarization at $x=0.15$. Combining all these results, we conclude that $Co_{1-x}Fe_xS_2$ is a tunable spin-polarization system where the conduction electron spin polarization can be controlled from −57% to 85%.

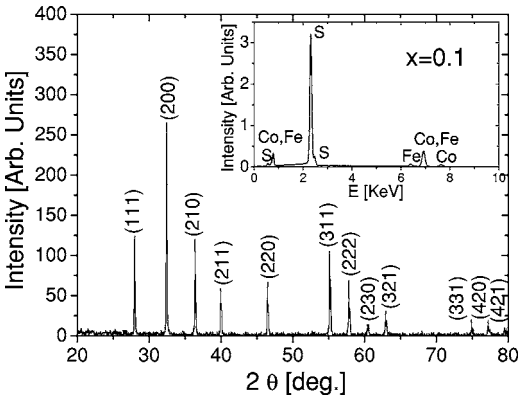

FIG. 1. X-ray powder diffraction from a representative ($x=0.10$) polycrystalline sample of $Co_{1-x}Fe_xS_2$. Inset: Energy dispersive spectroscopy on the same sample shown in the main panel. The energy of the electron beam was 20 kV.

II. EXPERIMENTAL CONSIDERATIONS

Bulk polycrystalline samples of $Co_{1-x}Fe_xS_2$ ($0<x<0.30$) were prepared by a three-stage process; liquid phase reaction, followed by solid-state heat treatment, then resulfurization. Consistent with previous literature,[59] we were unable to synthesize homogeneous substitutional solid solutions using standard solid-state reaction techniques. In our new three-step procedure, CoS_2 and FeS_2 powders (250 mg in total) were thoroughly ground and sealed in a quartz tube with 800 mg of S powder. The tube was subsequently evacuated to $<1\times10^{-6}$ Torr. The powder was then heated to 1000 °C for three days. This step is performed above or near the melting point of the sulfides to encourage formation of a homogeneous substitutional solution. After cooling to room temperature, the reaction product was ground and heated again with 150 mg S at 900 °C for seven days, to counteract the small amount of phase separation that occurs on cooling below the melting point. The resulting powder is significantly S deficient due to the high processing temperature. To obtain stoichiometric samples, the powder was then resulfurized with 150 mg S at 700 °C (a relatively low temperature), pressed into a pellet under 3×10^6 psi, and sintered with 120 mg S at 700 °C. The x-ray diffraction pattern of an $x=0.1$ sample is shown in Fig. 1 as an example. The data are consistent with the desired pyrite structure with no additional peaks due to secondary phases. The lattice parameters deduced from the (200) peak follow Vegard's law [see Fig. 2(a)] and the full width at half-maximum of the (200) peak is independent of x, as shown in Fig. 2(b). The latter point is particularly important as it demonstrates the formation of a homogeneous substitutional solid solution. Any phase separation into CoS_2 and FeS_2 (or Co and Fe rich regions) would

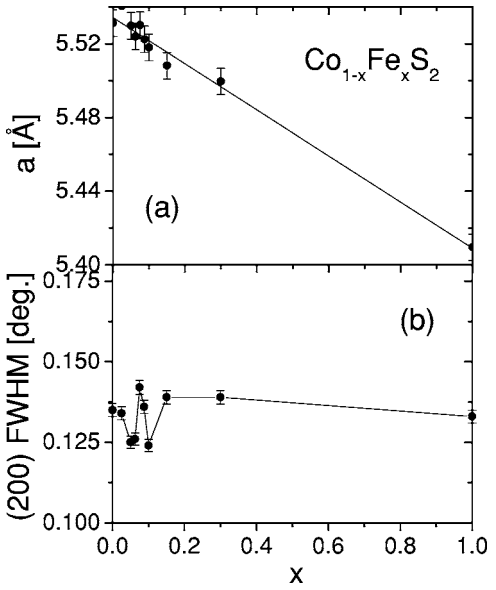

FIG. 2. Fe doping dependence of (a) the lattice parameter, a, determined from the position of the (200) x-ray diffraction peak, and (b) the full width at half-maximum of the (200) x-ray diffraction peak. The solid line in (a) demonstrates the adherence to Vegard's law.

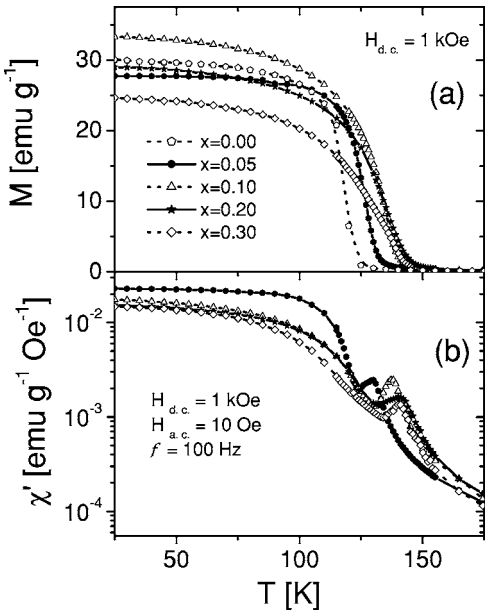

FIG. 3. Temperature dependence of (a) the dc magnetization, and, (b) the ac susceptibility, for $x=0.00$, 0.05, 0.10, 0.20, and 0.30. Magnetization data were taken in a static 1 kOe field, while the ac susceptibility was measured in a 1 kOe static field with a 10 Oe driving field at 100 Hz.

manifest itself as a broadening of these peak widths due to the existence of two overlapping, but unresolvable, peaks. Such behavior was indeed observed prior to optimization of the synthesis method. Energy dispersive spectroscopy (inset to Fig. 1) indicates a composition of $Co_{1-x}Fe_xS_{2.2}$, i.e., excess S, with no detectable impurities.

The dc and ac magnetic response, AMR, and heat capacity were measured in a Quantum Design Physical Property Measurement System in the temperature range $5\ \mathrm{K} < T < 300\ \mathrm{K}$ and in magnetic fields up to 90 kOe. The frequency and driving field for the ac susceptibility measurement were 100 Hz and 10 Oe, respectively. The magnetotransport measurements employed an ac excitation at 13.7 Hz in the temperature range $4.5\ \mathrm{K} < T < 300\ \mathrm{K}$. Magnetic fields were applied parallel to the sample plane and the current. The AMR measurements were performed with a rotator probe such that the field could be applied parallel or perpendicular to the measuring current. The relaxation technique was used to measure the heat capacity using a standard heat capacity puck (Quantum Design). The spin polarization of our samples was probed by the PCAR method, with both Pb and NbN tips, and fitted with the model of Strijkers *et al.*,[60] which is a modified form of the Blonder-Tinkham-Klapwijk (BTK) approach.[61] P was estimated by measurement of multiple contacts followed by extrapolation to $Z=0$, where Z is the dimensionless quantity used to describe the strength of the interfacial barrier.[60,61] Further details are provided with the discussion of the experimental results.

III. RESULTS AND DISCUSSION

A. Dc and ac magnetometry

The temperature dependence of the dc magnetization (M) and the in-phase ac susceptibility (χ') (in a static field of 1 kOe) was measured for ten different dopant levels ($0 < x < 0.3$). Five representative curves ($x=0.00$, 0.05, 0.10, 0.20, and 0.30) are shown in Fig. 3. The sudden loss of dc magnetization and the sharp peak in χ' near T_C demonstrate that CoS_2 ($x=0$) is close to exhibiting a first-order phase transition from FM to paramagnetic, as noted previously.[36,51–53,62] This sharp transition evolves into a more continuous smooth transition with increasing doping level, with $M(T)$ showing a "Brillouin-like" temperature dependence for $x > 0.05$. All samples show a peak in the ac susceptibility providing a measure of the Curie temperature (T_C), which we also determined more accurately with the heat capacity measurements discussed later (Sec. III C). The T_C determined by the two methods is shown in Fig. 4. The T_C from $\chi'(T)$ is about 4 K higher than the corresponding $C_p(T)$ result, independent of x.

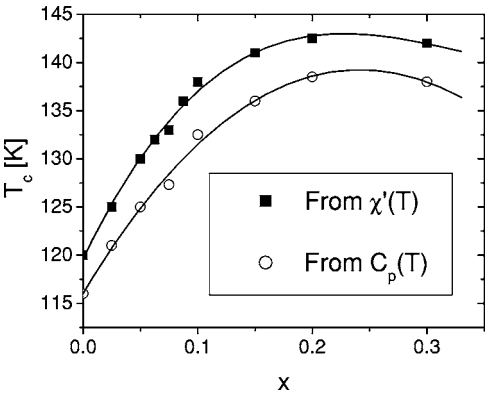

FIG. 4. Fe doping dependence of the Curie temperature determined from ac susceptibility (solid points) and heat capacity (open points). The solid lines are guides to the eye.

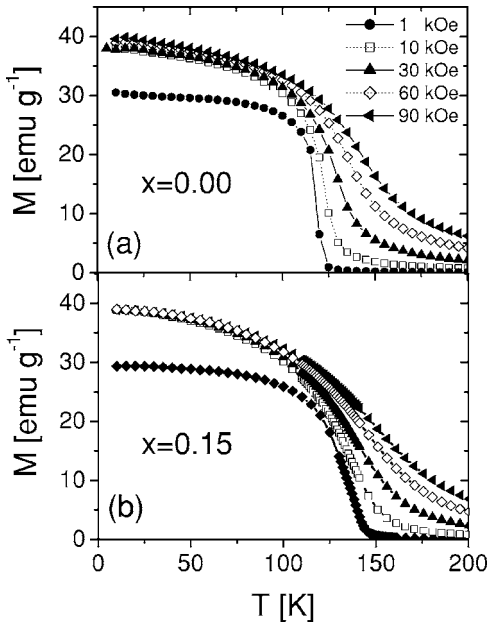

FIG. 5. Temperature dependence of the magnetization at (a) $x=0.00$, and (b) $x=0.15$, for applied dc magnetic fields of 1, 10, 30, 60, and 90 kOe.

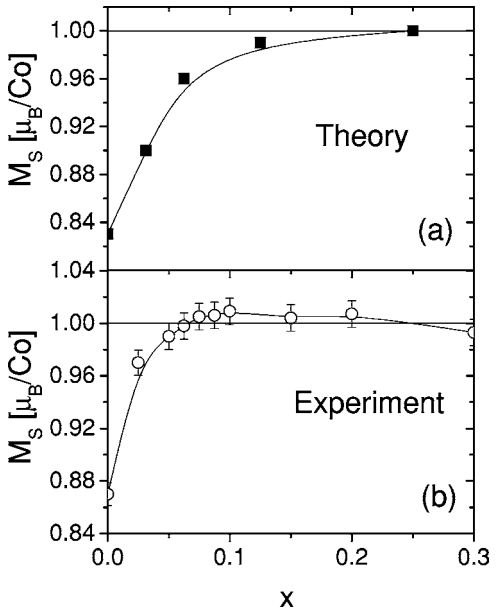

FIG. 6. Fe doping dependence of the saturation magnetization (in units of Bohr magnetons per Co ion) from (a) theoretical band structure calculations, and (b) experiment. The values in (b) explicitly assume zero magnetic moment on the Fe ions, as discussed in the text. The horizontal solid lines indicate the value of 1.0 μ_B/Co expected for a half-metal.

T_C initially increases with increasing Fe doping, achieving a maximum value at $x \approx 0.20$. At $x > 0.20$ the data are suggestive of a weak decrease with further increase in x. This nonmonotonic behavior agrees with the previous results of other groups,[41,52,57] and is quite counterintuitive. It is known that the Fe atoms are expected to have $S=0$ (they are $t_{2g}^6 e_g^0$ and FeS_2 is not ferromagnetic) meaning that this system is showing an enhancement of T_C with dilution by (presumably) nonmagnetic dopants. Although we have no conclusive interpretation of these data, it is worth noting that an increase in T_C with increasing disorder has been observed in recent dynamic mean field theory calculations in the disordered one band Hubbard model.[63]

The $M(T)$ curves of the $x=0$ and $x=0.15$ samples measured at different applied magnetic fields are shown in Fig. 5. As expected, we observe the broadening of the transition from FM to paramagnet in high magnetic fields. Consistent with prior work, the $x=0$ sample crosses over from a sharp transition in $M(T)$ at $H=0$, to a smooth transition at large field. Based on the magnetization at 10 K in a 90 kOe field, we obtained the saturation magnetization in units of Bohr magneton per Co ion as a function of x (Fig. 6). To do this, we explicitly assume zero moment on the Fe atoms, consistent with the aforementioned simple expectations and the results of our band structure calculations.[35] Recent Co NMR data provide further evidence that this assumption is valid.[64] The saturation magnetization per Co ion takes a noninteger value at $x=0.00$ (0.87 μ_B/Co), increases with x, and reaches 1.0 μ_B/Co at $x=0.07$, which is maintained up to $x=0.2$. The experimental values of M_S show remarkable agreement with the theoretical calculation, also shown in Fig. 6. The attainment of an M_S of an integer Bohr magneton per formula unit is a necessary but not sufficient condition for half metallicity. Because the electronic configurations of Co in CoS_2 and Fe in FeS_2 are $t_{2g}^6 e_g^1$ and $t_{2g}^6 e_g^0$, respectively, the expected M_S for the half-metallic $Co_{1-x}Fe_xS_2$ system is 1.0 μ_B/Co (derived from the single Co e_g electron). The measured M_S of 1.0 μ_B/Co for $0.07 < x < 0.3$ is therefore consistent with a half-metallic state. Figure 7 shows the field dependence of the sample magnetization for $x=0.00$, 0.05, 0.15, and 0.20 samples. All these samples show soft ferromagnetic behavior, i.e., the coercivity is very low ($\sim$10 Oe) and saturation is achieved in about 2 kOe. The inset to Fig. 7 shows the hysteresis loop of CoS_2 over the expanded field region from −90 kOe to 90 kOe. A small but finite slope exists at high field and results in a slight overestimation of M_S when the 90 kOe value is used. This could explain the measurement of saturation magnetizations slightly in excess of 1.0 μ_B/Co for $0.07 < x < 0.20$.

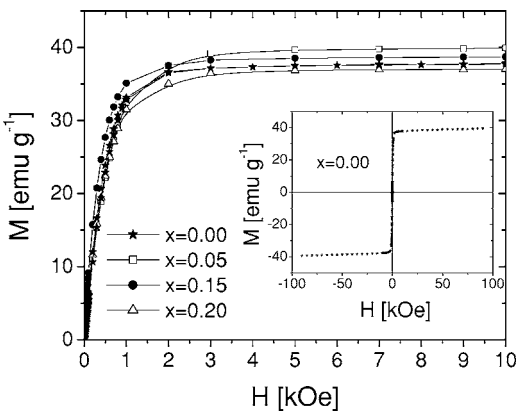

FIG. 7. Magnetization vs applied magnetic field (up to 10 kOe) for $x=0.00$, 0.15, 0.20, and 0.50. Inset: $x=0.00$ data in the expanded field region out to 90 kOe.

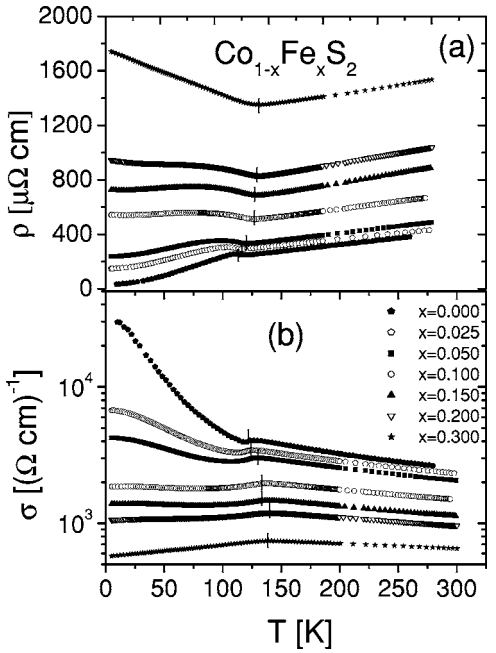

FIG. 8. Zero magnetic field temperature dependence of (a) the resistivity and (b) the conductivity for $x=0.000$, 0.025, 0.050, 0.100, 0.150, 0.200, and 0.300. The short vertical lines indicate the position of T_C.

B. Transport and magnetotransport

1. Zero field resistivity

The temperature dependence of the zero field electronic transport is shown in Fig. 8, which plots both the resistivity and conductivity (σ) of seven representative samples. $\rho(T)$ shows a very clear correlation between the electronic conduction and the magnetic ordering, the short vertical lines indicating the position of T_C. For all samples, the resistivity shows the typical linear dependence with T from 300 K down to T_C. Below T_C, the characteristics of the resistivity for the $Co_{1-x}Fe_xS_2$ system changes from a metallic-like temperature dependence (ρ increasing with T) to a semiconducting-like temperature dependence (ρ decreases with T) as x increases from 0 to 0.3. This is illustrated more clearly in Fig. 9, which plots the dependence of the low temperature (10 K) σ and $d\rho/dT$. (Note that this figure also plots the total DOS from band structure calculations and heat capacity measurements, and will be discussed in the next section.) The transition between the two regimes (i.e., the sign change in $d\rho/dT$) occurs at $x\approx 0.10$. It should be noted, however, that even at $x=0.3$, the apparent zero temperature extrapolation of the conductivity is finite [see Fig. 8(b)], meaning that all compositions are in fact metallic. A true $T=0$ MIT is expected to occur at higher x, as FeS_2 is known to be a semiconductor with a band gap of ~ 1 eV. It is therefore expected that at $x>0.30$, $\sigma(T=0)$ will reach zero and $d\rho/dT$ will change sign even at $T>T_C$. It is worth pointing out that the situation that occurs at $x>0.10$, i.e., a crossover from a metallic-like temperature dependence to an insulating-like temperature dependence on cooling through T_C, is extremely unusual. In fact, this behavior is exactly opposite to many systems of current interest.[65]

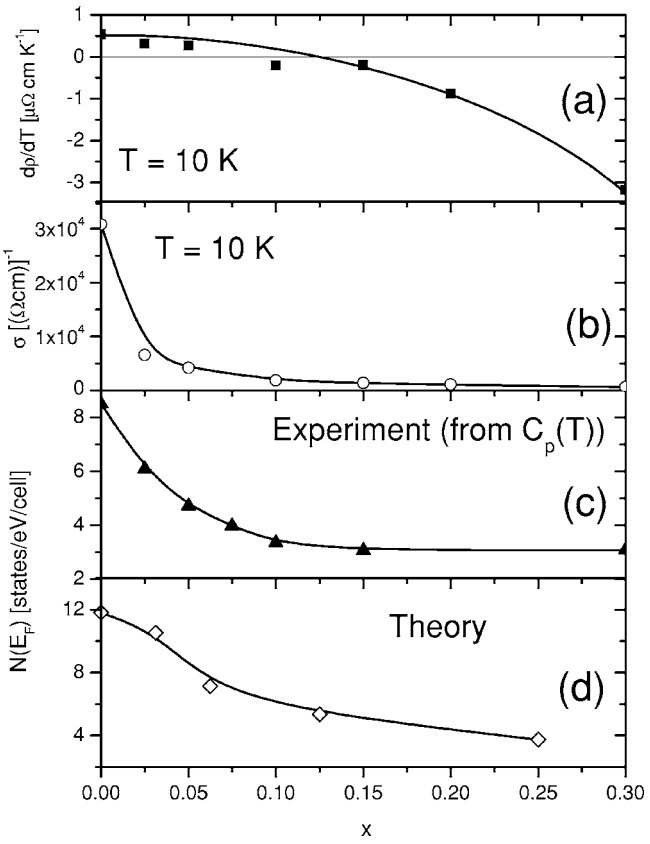

FIG. 9. Fe doping dependence of (a) $d\rho/dT$ at 10 K, (b) the 10 K conductivity, (c) the total (both spin orientations) density of states at the Fermi level extracted from the electronic contribution to the heat capacity below 60 K, and, (d) the total density of states from electronic band structure calculations.

We begin our discussion of the evolution of $\rho(T)$ with doping at $x=0.00$, which we have examined in detail in a previous publication.[36] Mazin[38] has previously pointed out that exotic transport effects are to be expected in this system due to the unusually large value of $dN(E)/dE$ at $E=E_F$. As discussed below, this, plus the known existence of E_F very close to the bottom of the conduction band[35–41] and the presence of disorder, will feature prominently in our explanations for the transport behavior. At $x=0.00$, a metallic-like $\rho(T)$ is found at $T>T_C$ and at low temperatures, but with a large anomaly in the resistivity at T_C. This anomaly takes the form of an increase in resistivity as the temperature is lowered through T_C, and was interpreted in our previous work as a spin-dependent band structure effect.[36] It is known, from previous theoretical work,[35–41] and our own calculations,[35] that E_F lies very low in the conduction band at $x=0.00$. The essential concept of our model is that as the temperature is lowered through T_C and the exchange splitting of the conduction bands takes place, the total (both spin channels) DOS decreases abruptly due to the fact that the minority spin DOS at E_F almost vanishes, i.e., one spin orientation barely contributes to the transport. This could occur due to E_F lying below the conduction band edge for the minority spins (a "true" half-metal) or below the mobility edge E_μ (a "transport" half-metal). In either case the reduction in the total

DOS at E_F results in a sharp decrease in the conductivity, and the "hump" in $\rho(T)$ just below T_C. For $x=0.00$, at temperatures just in excess of T_C, the proximity to a first-order FM to paramagnetic transition[36,51–53,62] means that a transition to a ferromagnetic state can be induced by large magnetic fields.[36] This results in the same exchange splitting that occurs on cooling through T_C in zero magnetic field, meaning that a positive magnetoresistance is observed, having the same magnitude as the increase in resistivity that occurs when cooling through T_C.[36] This MR, and its evolution with doping is discussed in detail below.

To explain qualitatively the variation in $\rho(T)$ at $T<T_C$ with increasing doping, specifically the evolution from a sharp peak in $\rho(T)$ at $x=0.00$ to a sign change in $d\rho/dT$ for $x>0.10$, we extend the spin-dependent band structure model previously developed for undoped CoS_2.[36] Again, our explanation hinges on the existence of a Fermi level very close to the conduction band edge, the presence of disorder (from random doping), and the significant size of the conduction band exchange splitting. Specifically, we propose that the point $x=0.10$, where $d\rho/dT$ (at $T<T_C$) changes sign [see Fig. 9(c)], is the point at which E_F falls below the mobility edge for the majority spin subband at $T<T_C$. Metallic behavior prevails at $T>T_C$, but at $T<T_C$, the exchange splitting of the conduction band results in a situation where the minority spins provide a negligible contribution to the transport, and even in the majority spin subband E_F lies just below E_μ, resulting in a semiconductor-like $\rho(T)$. As we will see later, the spin polarization measured by PCAR at these compositions is still $<100\%$. This could be due to a small contribution from thermally excited minority spins (the energy barrier for this excitation will be small), a limitation of the PCAR technique, which does not utilize ideally characterized interfaces, a problem with the interfaces of these sulfides, or materials defects such as grain boundaries or S interstitials. If x were increased further (beyond $x=0.30$) the Fermi level would eventually move below the majority spin subband (and therefore well below E_μ), resulting in a true zero temperature MIT and a $T=0$ extrapolation of the conductivity of zero.

2. Magnetoresistance

The behavior of the resistivity in magnetic fields up to 90 kOe is shown as a function of temperature in Fig. 10 (for $x=0.00$, 0.025, 0.05, 0.15, and 0.30) and as a function of field in Fig. 11 (for $x=0.00$, 0.05, and 0.30). Significant (10%–20%) MR effects are observed from temperatures just above T_C down to liquid helium. In discussing this data, we will again begin at $x=0.00$, which was discussed in a previous publication.[36] Figure 10(f) shows the 90 kOe MR extracted from the temperature sweeps shown in Fig. 10(a). Figure 11(a) shows corresponding field sweeps taken at three representative temperatures. A positive MR of approximately 8% occurs near T_C, due to the previously described spin-dependent band structure effect.[36] Essentially, the application of large magnetic fields emulates the reduction in total DOS at E_F obtained when cooling below T_C in zero applied field, i.e., the resistivity is controlled by the magnetization. This positive MR in the vicinity of T_C is observed at all x values,

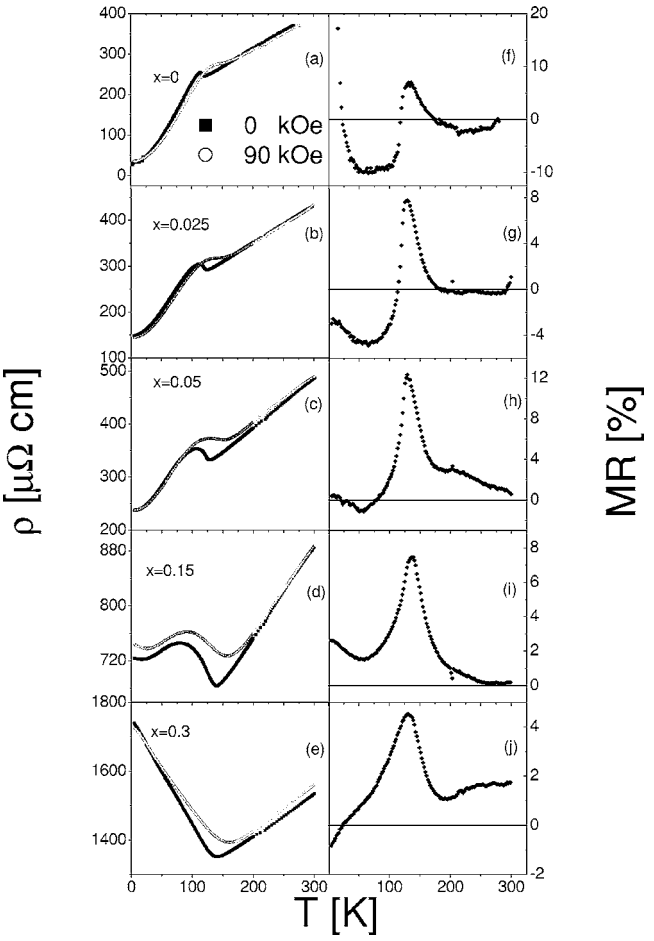

FIG. 10. Temperature dependence of the zero field (solid points) and 90 kOe (open points) resistivity (left panel) and the 90 kOe magnetoresistance ratio (right panel) for $x=0.000$, 0.025, 0.050, 0.150, and 0.300. The magnetoresistance ratio is defined as $[\rho(H)-\rho(0)]/\rho(0)$.

as shown in Figs. 10(g)–10(j). The influence of doping is illustrated more clearly in Fig. 12 which shows the x dependence of the MR at $T=T_C$, as well as the increase in ρ that occurs on cooling below T_C in zero field (see the figure caption for a precise definition). We propose that the spin-dependent band structure argument used to explain the positive MR near T_C in CoS_2 is also applicable at $x>0.00$, i.e., that the magnetization controls the resistivity. As shown in Fig. 12, increasing x leads to an increase in the magnitude of the positive MR near T_C, from 7% at $x=0.00$ to 12% at $x=0.05$. This is accompanied by a concomitant increase in the change in resistivity that occurs on cooling below T_C in zero magnetic field, from 8% at $x=0.00$ to 14% at $x=0.05$. (This quantity is plotted as ΔR in Fig. 12, and is defined in the figure caption). At $x>0.05$ the simple correlation between the two quantities plotted in Fig. 12 no longer holds, no doubt due to the change in the transport mechanism, as previously discussed, i.e., the simple metallic behavior is lost and a straightforward connection between conductivity and total DOS at E_F can no longer be made.

Examining Fig. 10(f) further, it is clear that two other MR contributions can be observed. At the lowest temperatures, a

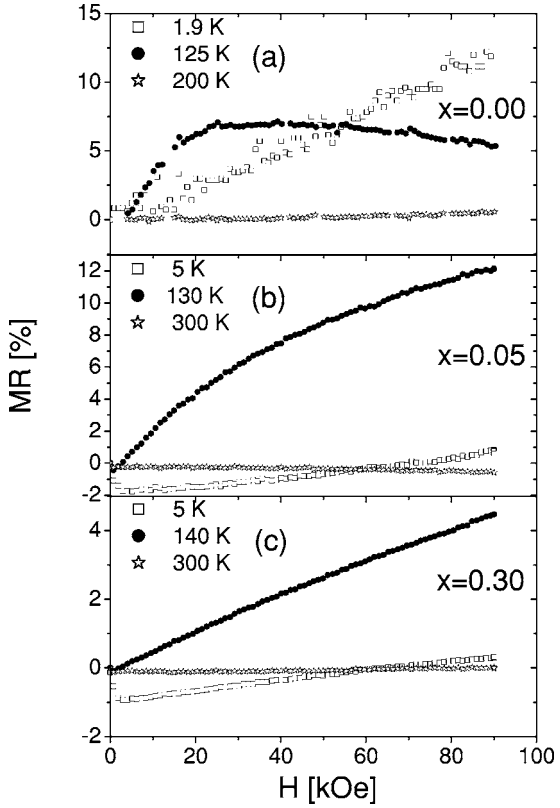

FIG. 11. Magnetic field dependence of the MR ratio (see previous caption for a definition) for (a) $x=0.00$, (b) $x=0.05$, and (c) $x=0.30$. In each case the data were taken at three representative temperatures; the lowest temperature (5 K), high temperature (200 or 300 K), and close to T_C.

conventional positive MR is observed, as is typically the case in metals. At temperatures intermediate between helium and T_C, a negative MR is observed. This is due to the usual field-induced suppression of electron-magnon scattering in FM metals[66] and provides us with a useful probe of the conduction electron spin polarization.[35] These two MR contributions, and their doping dependence, will now be discussed in turn.

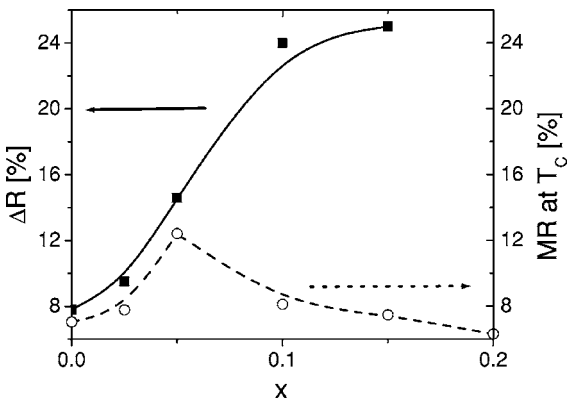

FIG. 12. Fe doping dependence of the increase in resistivity that occurs on cooling through T_C (ΔR, solid points) and the 90 kOe MR ratio at T_C (open points). (ΔR is defined as the difference between the linear extrapolation of the high temperature ($T>T_C$) resistivity and the measured zero field resistivity at the peak. The percentage value is calculated by the difference over the linear extrapolation value.)

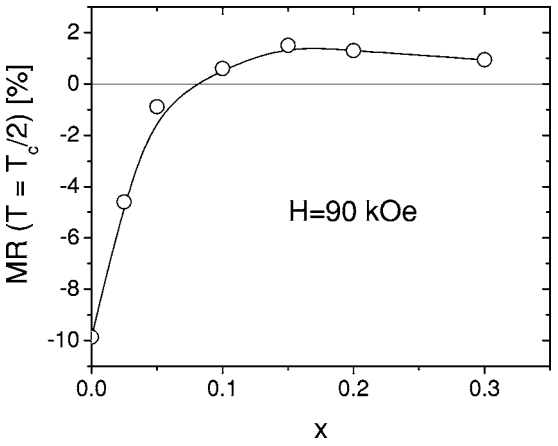

FIG. 13. Fe doping dependence of the 90 kOe MR at $T_C/2$. This temperature was chosen as representative of the region where the negative MR dominates.

As shown in Figs. 10(f) to 10(j) the low-temperature positive MR is rapidly suppressed upon doping. At $x=0.00$, this MR contribution dominates below approximately 25 K, diverging as $T\rightarrow 0$. We interpret this as being due to the conventional positive MR effect usually observed in metals at low T. Such MR is sensitive to the carrier mobility, naturally explaining the drastic reduction in low T positive MR as the doping increases, the conductivity falls, and the MIT is approached.

The final mechanism contributing to the $x=0.00$ MR(T) [Fig. 10(f)] is the field-induced suppression of electron-magnon scattering, as is usually found in FM metals.[66] This contribution dominates the $x=0.00$ MR at $20\ \mathrm{K}<T<115$ K. In this mechanism large applied fields suppress the excitation of magnons, eliminating electron- (one-[67–69]) magnon spin-flip scattering processes and enhancing the conductivity, i.e., a negative MR occurs. At low temperatures, few magnons are excited and the negative MR is therefore small. As the temperature approaches T_C, the ferromagnetism is lost and the effect again disappears. At intermediate temperatures ($\approx T_C/2$), however, the negative MR from the field-induced suppression of electron-magnon scattering is maximized, and dominates MR(T). As shown in Figs. 10(f) to 10(j) this electron-magnon contribution to the MR evolves in an interesting way with increasing doping. This is illustrated more clearly in Fig. 13, which plots the 90 kOe MR at $T=T_C/2$ from $x=0.00$ to 0.30. The magnitude of the negative MR decreases rapidly with increasing x, reaching zero at $x\approx 0.07$. This is further strong evidence for increasing spin polarization with Fe doping. In a system with 100% spin polarization spin-flip scattering events are completely suppressed due to the absence of available minority spin states to scatter into. The negative MR due to field suppression of electron-magnon scattering therefore disappears with increasing spin polarization. It is important to point out that our negative MR vanishes near $x\approx 0.07$, consistent with the data of Fig. 6, which show that $x=0.07$ is the point at which

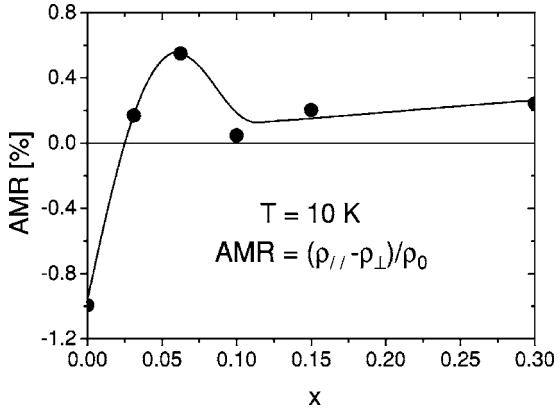

FIG. 14. Fe doping dependence of the AMR ratio (defined in the text) at $T=5$ K and $H=80$ kOe.

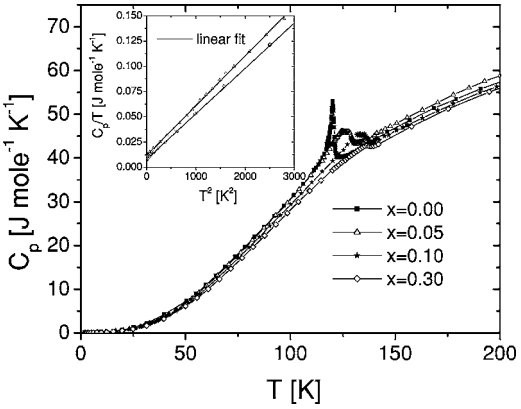

FIG. 15. Temperature dependence of the (zero magnetic field) specific heat at $x=0.00$, 0.05, 0.10, and 0.30. Inset: C_p/T vs T^2 for $x=0.05$ and 0.30. The solid lines are linear fits.

the system attains a magnetization of 1.0 μ_B/Co, consistent with entry into a half-metallic state. The overall situation is quite analogous to that observed by Watts *et al.* in CrO_2,[70] where a crossover from positive to negative MR occurs with increasing T, the crossover temperature coinciding with the point at which spin-flip scattering becomes evident in $\rho(T)$. Note that the small positive MR at $x \geq 0.1$ in Fig. 13 is likely due to a small contribution from the large positive peak in MR(T) that is centered on T_C [see Fig. 10(i)].

3. Anisotropic magnetoresistance (AMR)

Another probe of the conduction electron spin polarization is provided by the AMR, which is defined as

$$\mathrm{AMR} = \frac{\rho_{\parallel} - \rho_{\perp}}{\rho_0}, \tag{4}$$

where $\rho_{\parallel}$ and $\rho_{\perp}$ are the respective resistivities with the current parallel and perpendicular to the magnetization, and ρ_0 is the zero field resistivity. The doping dependence of this AMR is shown in Fig. 14. At $x=0.00$ a negative AMR is observed with a magnitude ($\sim 1.0\%$) typical for conventional ferromagnetic metals.[71] Higher doped samples exhibit positive AMR, indicating a sign change between $x=0.00$ and 0.03. Although the AMR of ferromagnetic metals is notoriously difficult to treat theoretically, several theories have been developed. Most notably, the comprehensive work by Potter and McGuire[71] points out that the sign of the AMR is controlled by the sign of the spin polarization, i.e., FMs where the conduction is dominated by minority spin electrons should have AMR <0 ($\rho_{\perp} > \rho_{\parallel}$) and systems dominated by majority spin electrons should have AMR >0 ($\rho_{\parallel} > \rho_{\perp}$). Within this framework, the data of Fig. 14 can be simply interpreted as a sign change in P (from negative to positive) as x increases from $x=0.00$ to 0.03. In other words, the spin polarization apparently changes sign from negative to positive prior to attaining large positive values at $x \geq 0.07$. This result is completely consistent with our band structure calculations;[35] CoS_2 was predicted to be a minority spin FM, crossing over to a majority spin FM with Fe doping, eventually attaining $P=100\%$ at $x=0.25$. Theory and experiment are therefore in qualitative agreement, although the exact x value for the sign change in P and the onset of high positive P are in disagreement. This will be discussed later. As a final comment on these data, note that the inability of PCAR to determine the sign of the spin polarization makes the sensitivity of the AMR to the sign of P all the more valuable.

C. Heat capacity

In order to probe the thermodynamic properties as a function of the spin polarization, we measured the temperature dependence of the specific heat (C_p) as a function of Fe doping. These measurements should provide important information on the evolution of the electronic and magnetic contributions to the heat capacity with Fe doping, and therefore spin polarization. Figure 15 shows the zero field $C_p(T)$ of $Co_{1-x}Fe_xS_2$ ($x=0.00$, 0.05, 0.10, and 0.30) from 1.8 to 200 K. Following the standard analysis of the heat capacity of FM materials, electronic, lattice, and magnetic contributions must be taken into account. At low temperatures, based on the free electron gas and Debye model, C_p can be expressed as

$$C_P(T) = \frac{\pi^2}{3} k_B^2 T N(E_F) + 234\left(\frac{T}{\Theta_D}\right)^3 n k_B + C_p^{mag}(T), \tag{5}$$

where k_B, $N(E_F)$, Θ_D, and n are the Boltzmann constant, the total DOS at E_F, the Debye temperature, and the number density of ions, respectively. In our case, the magnetic contribution was found to be significant only near T_C, as discussed below. Following Eq. (5), C_p/T was plotted versus T^2 (see inset to Fig. 15 for two examples at $x=0.05$ and 0.30) to extract $N(E_F)$ and Θ_D. Note that straight-line behavior is observed in both cases (at $T<60$ K), implying that no significant low temperature magnetic contribution is required to fit the data, i.e., there is no visible $T^{3/2}$ contribution from magnon excitations.[72] In order to shed further light on this issue we made an estimate of the expected value for δ using the spin wave stiffness, $D=110$ meV Å^2, previously measured for undoped CoS_2 by neutron scattering.[73] Using simple relations for cubic systems, we obtain $\delta = 0.88$ mJ/mole K$^{-5/2}$, considerably larger than our expected detection limit. Moreover, by remeasuring the heat capacity

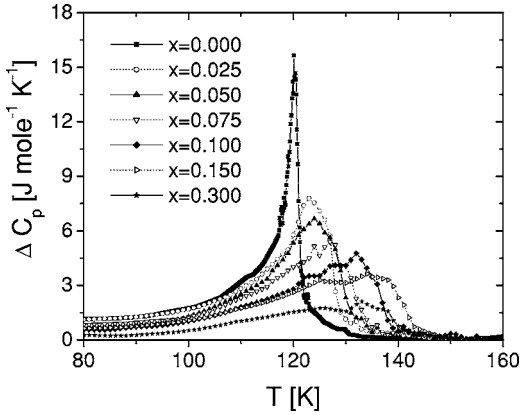

FIG. 16. Temperature dependence of the magnetic contribution to the zero magnetic field specific heat (ΔC_p) at $x=0.000$, 0.025, 0.050, 0.075, 0.100, 0.150, and 0.300. The subtraction of other contributions is discussed in the text.

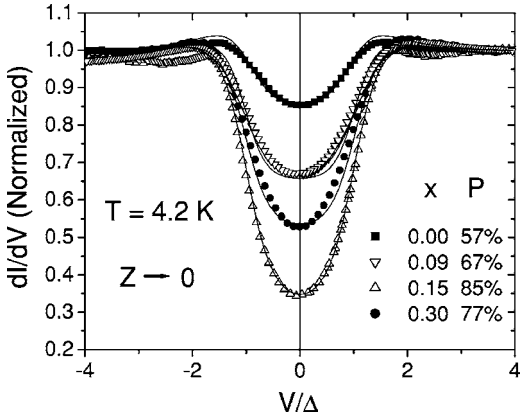

FIG. 17. PCAR conductance voltage curves for $x=0.00$, 0.09, 0.15, and 0.30 at 4.2 K in zero magnetic field. The conductance is normalized to the normal state value (at a voltage of +4.0 V/Δ), while the voltage is normalized to the superconducting gap voltage. The solid lines are fits to the model described in the text with fitting parameters; $x=0.00$, $P=57\%$, $Z=0.00$; $x=0.09$, $P=56\%$, $Z=0.08$; $x=0.15$, $P=80\%$, $Z=0.28$; $x=0.30$, $P=73\%$, $Z=0.09$. The P values cited in the table in the lower right corner of the figure are the $Z=0$ extrapolations.

in a large magnetic field of 90 kOe we should be able to suppress any low-temperature magnon contribution to the heat capacity. The measurements revealed a reduction in heat capacity of at most 6% at 1.8 K, compared to an anticipated decrease of about 15% using the expected δ value and assuming 90 kOe is sufficient to completely suppress magnon excitation at these temperatures. In summary, although we can provide no obvious explanation, it is intriguing that these highly polarized ferromagnets apparently show no heat capacity contribution from magnons.

As shown in Fig. 9(c), the DOS at E_F extracted from $C_p(T)$ decreases with increasing doping level, in quite reasonable agreement with the results of our band structure calculations. These data are consistent with Figs. 8, 9(a), and 9(b), showing a decrease in conductivity and crossover to a semiconducting-like $\rho(T)$ with increasing doping. The Debye temperatures extracted from the low-temperature $C_p(T)$ versus T^2 curves vary only weakly with doping, as expected, having values in the range 480 K to 500 K. The weak observed increase in Debye temperature with increasing x can be accounted for by the increase in melting point.

At higher temperatures (above 60 K), obvious magnetic contributions to the heat capacity occur, most notably the large "lambda" anomalies occurring near T_C. We fitted the $C_p(T)$ curves from 5 to 200 K using Eq. (5), in order to separate the magnetic contributions near T_C from the lattice and electronic contributions. Consistent with the findings mentioned above, we did not include any low-temperature magnon contribution. In this fitting procedure we used the electronic contribution previously determined from the C_p versus T^2 curves at low T, and allowed Θ_D to vary. The Debye temperatures obtained in this manner are within 2 K of those obtained from low-temperature fitting. The magnetic contributions to $C_P(T)$ in $Co_{1-x}Fe_xS_2$ ($x=0.000$, 0.025, 0.050, 0.075, 0.100, 0.150, and 0.300) are shown in Fig. 16. The peak in the magnetic contribution to the heat capacity is pushed to higher temperatures with increasing doping (due to the increase in T_C), and becomes increasingly smaller in magnitude. The decrease in peak size is presumably due to the FM-paramagnet transition becoming increasingly more second-order with doping. As mentioned previously, it is known that undoped CoS_2 lies close to the tricritical point separating first and second order magnetic transitions, and that Fe doping moves the system away from this special point.

D. Point contact Andréev reflection (PCAR)

PCAR measurements were employed as a more direct measure of the conduction electron spin polarization. Figure 17 shows the conductance G (normalized to the normal state value) versus the applied voltage V (normalized to the superconducting gap voltage) for $Co_{1-x}Fe_xS_2$ samples with $x=0.00$, 0.09, 0.15, and 0.30. Note that results were obtained with two different tip materials (Pb and NbN) and in each case multiple contacts were measured on the same sample. A modified version of the BTK model[61] was used to analyze the experimental $G(V)$ curves and extract P.[60] The interfacial scattering is modeled via a delta function potential at the interface with a dimensionless height Z.[60,61] All the curves can be fitted very well using three adjustable parameters: the spin polarization, the superconducting gap value, and the interfacial scattering strength Z. The lines in the figure are the results of the fits. (The fitting parameters are provided in the figure caption.) Even before any model-dependent fitting it is clear from the extent of the subgap conductance suppression that P increases rapidly with increasing doping. At $x=0.15$ the normalized conductance at zero bias reaches a value of only 0.33, corresponding to 84% spin polarization within the simplest Andréev reflection treatment.[14] The more complete fitting procedure described above results in a value of 85%. This fitting was applied to numerous point contacts and the extracted P values are plotted as a function of the Z value for the particular contact in Fig. 18. The P values decrease with increasing Z, as observed previously for PCAR measure-

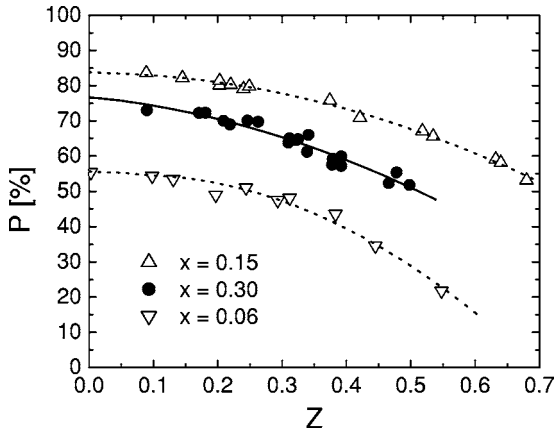

FIG. 18. Dependence of the spin polarization on the interfacial barrier strength parameter Z, for $x=0.06$, 0.15, and 0.30. The lines are guides to the eye. $T=4.2$ K.

ments on other highly polarized ferromagnets.[15,18] Although the exact mechanism for this decrease in P with increasing Z is not known (it does not occur in the planar geometry, where CrO_2 has been demonstrated to have $P=100\%$ independent of Z),[29] extrapolation to $Z=0$ is thought to yield the intrinsic P value. (For the case of the CrO_2 PCAR measurements the $Z=0$ extrapolation[15] agrees very well with the planar Andréev and Meservey-Tedrow data,[29] further evidence that this approach is valid). In our case the $Z\rightarrow 0$ extrapolations vary only slightly from the P values extracted from the $G(V)$ curves at the smallest Z measured.

Figure 19 compares the Fe doping dependence of the $Z\rightarrow 0$ extrapolation of P with the results of our band structure calculations. The experimental values [Fig. 19(b)] show a relatively weak doping dependence up to $x=0.07$ at which point the spin polarization increases rapidly, reaching a maximum of 85% at $x=0.15$. As x is increased further the spin polarization falls. Figure 19(a) shows the theoretical result from our band structure calculations. Note that, to allow a more direct comparison with experiment, the *magnitude* of the theoretical spin polarization is plotted, the PCAR measurement being insensitive to the sign of P. The first two doping values plotted on Figure 19(a), actually have negative P (minority spin). The decrease in magnitude with initial doping, followed by the sharp increase at $x=0.07$, therefore reflect the sign change in P. It is important to recall that our AMR measurements, which we believe *are* sensitive to the sign of P, suggest that the undoped $x=0.00$ sample has negative P. The overall agreement between experiment and theory is therefore quite reasonable; theory predicts a polarization of -75% at $x=0.00$, crossing zero at $x=0.07$ and achieving $P=100\%$ at $x=0.25$. Our experimental value is -57% at $x=0.00$, crossing zero around $x=0.03$ and achieving $P=85\%$ at $x=0.15$. Note that the point at which the experimental spin polarization values begin to increase sharply and a highly polarized state is entered ($x=0.07$), correlates very well with the point at which a saturation magnetization of 1.0 μ_B/Co ion is achieved ($x=0.07$) and the spin-flip scattering contribution to the high field MR vanishes ($x=0.07$). Together with the PCAR data these results must be taken as strong evidence for the existence of very highly spin-polarized conduction electrons in this composition range.

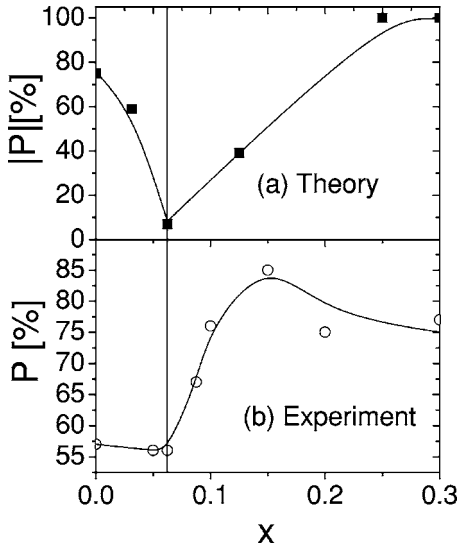

FIG. 19. Fe doping dependence of (a) the magnitude of the spin polarization from the band structure calculations, and (b) the spin polarization extracted from PCAR in the $Z=0$ limit. $T=4.2$ K. The solid vertical line denotes the point at which the theoretical polarization changes sign.

At this stage, it is important to contrast our results to those of Cheng *et al.* on single crystal $Co_{1-x}Fe_xS_2$.[58] In that work unexpectedly low spin polarizations ($<61\%$) were observed, with a very weak dependence on doping. As pointed out by the authors of that study the samples investigated exhibited S deficiency of up to 10% as well as significant Te impurities. Given the large spin polarizations we have observed in polycrystalline $Co_{1-x}Fe_xS_2$ in the absence of any S deficiency and the strong dependence on Fe doping, it is likely that the lower spin polarization observed in the prior work arose due to S deficiency. (Although it is not completely clear why S deficiency has a negative impact on P, we can make the general statement that when E_F lies so close to the bottom of the conduction band, small changes in band structure could have a significant influence on P.) We believe that the S diffusion coefficient will be much larger in our samples as it is known that grain boundary diffusion is orders of magnitude faster than the conventional substitutional mechanisms.[74] It is therefore easier to avoid S deficiency in polycrystalline materials or thin films, than in bulk single crystals. As discussed below, we have, however, been able to fabricate stoichiometric single crystals by a variant of the standard vapor transport process. The results will be published elsewhere.[75]

Despite the overall qualitative agreement between theory and experiment, and the demonstration of compositionally tunable high spin polarization, notable discrepancies between theory and experiment do exist. The absence of the initial decrease in the experimental $P(x)$ curve, the saturation of P at $<100\%$ (i.e., the absence of truly half-metallic behavior) and the disagreement with theory on the x values for the sign reversal in P and the attainment of large P values, are all problematic. There are a number of possible sources of dis-

crepancy. First and foremost, as detailed in Sec. I, there are several definitions of spin polarization, depending on the specific situation.[7] The theoretical data of Fig. 19(a) show the calculated DOS spin polarization using the definition in Eq. (1). However, the PCAR measurements probe the polarization of a current, with the definition given in Eq. (3) being the relevant one.[7] It is therefore clear that our experimental data are only directly comparable to the calculations in the case where the spin dependence of the Fermi velocity is small. This is likely the source of the discrepancies between theory and experiment at low x values. In particular, we do not observe P values close to zero near $x=0.05$, which can be attributed to the spin dependence of the Fermi velocity.[76] Second, all of our characterization data are consistent with the samples having a random distribution of Co and Fe atoms. This is in contrast to the band structure calculations, which require the use of supercells, and therefore model ordered alloys. The work of Mazin[38] suggests that this is not in fact a significant source of error, as the virtual crystal approximation and the supercell approach give similar results. Another factor that should be considered is the limitations of the PCAR technique, which suffers from the disadvantage of the use of a poorly characterized interface between tip and sample. Finally, it is possible that the measured spin polarization being less than 100% is due to deficiencies with the structural quality of the samples. We used extreme caution to ensure that S deficiency was avoided and it is in fact possible that excess S is present, either at the grain boundaries and/or surface, or as S interstitials. Either of these could reduce the spin polarization. The samples used in this study are also polycrystalline and it is unclear what effect the presence of grain boundaries will have on the measured spin polarizations. Stoichiometric single crystals of high structural perfection are currently being grown in our laboratory by a variant of the standard vapor transport method. Future work will involve a full investigation of the effect of S stoichiometry on the spin polarization, transport, and magnetic properties of $Co_{1-x}Fe_xS_2$ single crystals.

IV. SUMMARY AND CONCLUSIONS

In summary, we have demonstrated the feasibility of a simple scheme for engineering high spin polarization in $Co_{1-x}Fe_xS_2$ by alloy control of the position of the Fermi level. A combination of indirect probes such as the saturation magnetization, anisotropic magnetoresistance, and the spin-flip scattering contribution to the magnetoresistance, along with direct measurement by point contact Andréev reflection and theoretical band structure calculations, have provided a consistent picture in which the spin polarization can be tuned in the range $-57\% < P < 85\%$. The evolution of the magnetic, transport, and thermodynamic properties with Fe doping (and therefore spin polarization) have been investigated in detail. The transport properties in particular are rather exotic, with many features that can be interpreted in terms of the spin-dependent band structure of the material. The demonstration of compositionally tunable spin polarizations offers great opportunities for fundamental investigation of heterostructured spintronic devices and is planned for future work. Although the work presented here deals with a material with a Curie temperature of only 150 K, ruling out room temperature applications, it does demonstrate the feasibility of Fermi level control as a general means to tune spin polarization in ferromagnetic alloys. It will be interesting to see if other material combinations (with higher Curie temperatures) can be identified as possible candidates for this approach.

ACKNOWLEDGMENTS

Work at UMN was supported by the NSF MRSEC under DMR-0212302. PCAR measurements at Johns Hopkins were supported by NSF DMR-0080031. K. U. and R. M. W. acknowledge financial support from NSF DMR-0325218. Work at Harvey-Mudd was supported by a grant from the Parsons foundation. We would like to thank P. A. Crowell, W. G. Moulton, M. J. R. Hoch, and I. I. Mazin for valuable discussions.

*Corresponding author.

[1] S. A. Wolf, D. D. Awschalom, R. A. Buhrman, J. M. Daughton, S. von Molnar, M. L. Roukes, A. Y. Chtchelkanova, and D. M. Treger, Science **294**, 1488 (2001).

[2] J. B. Kortright, D. D. Awschalom, J. Stohr, S. D. Bader, Y. U. Idzerda, S. S. P. Parkin, I. K. Schuller, and H.-C. Siegmann, J. Magn. Magn. Mater. **207**, 7 (1999).

[3] M. N. Baibich, J. M. Broto, A. Fert, F. Nguyen Van Dau, F. Petroff, P. Etienne, G. Creuzet, A. Friederich, and J. Chazelas, Phys. Rev. Lett. **61**, 2472 (1986).

[4] B. Dieny, V. S. Speriosu, S. S. P. Parkin, B. A. Gurney, D. R. Wilhoit, and D. Mauri, Phys. Rev. B **43**, 1297 (1997).

[5] G. Grynkewich, J. Åkerman, P. Brown, B. Butcher, R. W. Dave, M. DeHerrera, M. Durlam, B. N. Engel, J. Janesky, S. Pietambaram, N. D. Rizzo, J. M. Slaughter, K. Smith, J. J. Sun, and S. Tehrani, MRS Bull. **29**, 11 (2004).

[6] J. S. Moodera and G. Mathon, J. Magn. Magn. Mater. **200**, 248 (1999).

[7] I. I. Mazin, Phys. Rev. Lett. **83**, 1427 (1999).

[8] J.-H. Park, E. Vescovo, H.-J. Kim, C. Kwon, R. Ramesh, and T. Venkatesan, Nature (London) **392**, 794 (1998); Phys. Rev. Lett. **81**, 1953 (1998).

[9] K. P. Kamper, W. Schmitt, G. Guntherodt, R. J. Gambino, and R. Ruf, Phys. Rev. Lett. **59**, 2788 (1987).

[10] S. A. Morton, G. D. Waddill, S. Kim, I. K. Schuller, S. A. Chambers, and J. G. Tobin, Surf. Sci. **513**, L451 (2002).

[11] R. Meservey and P. M. Tedrow, Phys. Rep. **238**, 173 (1994).

[12] M. J. M. de Jong and C. W. J. Beenaker, Phys. Rev. Lett. **74**, 1657 (1995).

[13] S. K. Upadhyay, A. Palanisami, R. N. Louie, and R. A. Buhrman, Phys. Rev. Lett. **81**, 3247 (1998).

[14] R. J. Soulen, J. M. Byers, M. S. Osofsky, B. Nadgorny, T. Am-

brose, S. F. Cheng, P. R. Broussard, C. T. Tanaka, J. Nowak, J. S. Moodera, A. Barry, and J. M. D. Coey, Science **282**, 85 (1998); R. J. Soulen, M. S. Osofsky, B. Nadgorny, T. Ambrose, P. Broussard, S. F. Cheng, J. Byers, C. T. Tanaka, J. Nowak, J. S. Moodera, G. Laprada, A. Barry, and J. M. D. Coey, J. Appl. Phys. **85**, 4589 (1999).

[15] Y. Ji, G. J. Strijkers, F. Y. Yang, C. L. Chien, J. M. Byers, A. Anguelouch, G. Xiao, and A. Gupta, Phys. Rev. Lett. **86**, 5585 (2001).

[16] A. Anguelouch, A. Gupta, G. Xiao, D. W. Abraham, Y. Ji, S. Ingvarsson, and C. L. Chien, Phys. Rev. B **64**, 180408 (2001).

[17] B. Nadgorny, I. I. Mazin, M. Osofsky, R. J. Soulen, P. Broussard, R. M. Stroud, D. J. Singh, V. G. Harris, A. Arsenov, and Y. Mukovskii, Phys. Rev. B **63**, 184433 (2001).

[18] Y. Ji, C. L. Chien, Y. Tomioka, and Y. Tokura, Phys. Rev. B **66**, 012410 (2002).

[19] S. K. Clowes, Y. Miyoshi, Y. Bugoslavsky, W. R. Branford, C. Grigorescu, S. A. Manea, O. Monnereau, and L. F. Cohen, Phys. Rev. B **69**, 214425 (2004).

[20] L. J. Singh, Z. H. Barber, Y. Miyoshi, Y. Bugoslavsky, W. R. Branford, and L. F. Cohen, Appl. Phys. Lett. **84**, 2367 (2004).

[21] For broad reviews, see: C. M. Fang, G. A. de Wijs, and R. A. de Groot, J. Appl. Phys. **91**, 8340 (2002); W. E. Pickett and J. S. Moodera, Phys. Today **54**, 39 (2001).

[22] A. M. Bratkovsky, Appl. Phys. Lett. **72**, 2334 (1998).

[23] M. Bowen, M. Bibes, A. Barthelemy, J.-P. Contour, A. Anane, Y. Lemaitre, and A. Fert, Appl. Phys. Lett. **82**, 233 (2003).

[24] G. Hu and Y. Suzuki, Phys. Rev. Lett. **89**, 276601 (2002).

[25] A. Gupta and J. Z. Sun, J. Magn. Magn. Mater. **200**, 24 (1999).

[26] R. Fiederling, M. Kelm, G. Reuscher, W. Ossau, G. Schmidt, A. Waag, and L. W. Molenkamp, Nature (London) **402**, 787 (1999).

[27] Y. Ohno, D. K. Young, B. Beschoten, F. Matsukura, H. Ohno, and D. D. Awschalom, Nature (London) **402**, 791 (1999).

[28] G. Schmidt, D. Ferrand, L. W. Molenkamp, A. T. Filip, and B. J. van Wees, Phys. Rev. B **62**, R4790 (2000).

[29] J. S. Parker, S. M. Watts, P. G. Ivanov, and P. Xiong, Phys. Rev. Lett. **88**, 196601 (2002).

[30] Y. S. Dedkov, U. Rudiger, and G. Guntherodt, Phys. Rev. B **65**, 064417 (2002).

[31] J. G. Braden, J. S. Parker, P. Xiong, S. H. Chun, and N. Samarth, Phys. Rev. Lett. **91**, 056602 (2003).

[32] P. A. Dowben and S. J. Jenkins, in *Frontiers in Magnetic Materials*, edited by A. V. Narlikar (Springer-Verlag, Berlin, 2005), p. 295.

[33] R. Skomski and P. A. Dowben, Europhys. Lett. **58**, 544 (2002).

[34] H. Itoh, T. Ohsawa, and J. Inoue, Phys. Rev. Lett. **84**, 2501 (2000).

[35] L. Wang, K. Umemoto, R. M. Wentzcovitch, T. Y. Chen, C. L. Chien, J. Checkelsky, J. Eckert, E. D. Dahlberg, and C. Leighton, Phys. Rev. Lett. **94**, 056602 (2005).

[36] L. Wang, T. Y. Chen, and C. Leighton, Phys. Rev. B **69**, 094412 (2004).

[37] G. L. Zhao, J. Callaway, and M. Hayashibara, Phys. Rev. B **48**, 15781 (1993).

[38] I. I. Mazin, Appl. Phys. Lett. **77**, 3000 (2000).

[39] S. K. Kwon, S. J. Youn, and B. I. Min, Phys. Rev. B **62**, 357 (2000).

[40] T. Shishidou, A. J. Freeman, and R. Asahi, Phys. Rev. B **64**, 180401 (2001).

[41] K. Ramesha, R. Seshadri, C. Ederer, T. He, and M. A. Subramanian, Phys. Rev. B **70**, 214409 (2004).

[42] D. Orgassa, H. Fujiwara, T. C. Schulthess, and W. H. Butler, Phys. Rev. B **60**, 13237 (1999).

[43] C. T. Tanaka, J. Nowak, and J. S. Moodera, J. Appl. Phys. **86**, 6239 (1999).

[44] B. Ravel, J. O. Cross, M. P. Raphael, V. G. Harris, R. Ramesh, and V. Saraf, Appl. Phys. Lett. **81**, 2812 (2002).

[45] G. Kirczenow, Phys. Rev. B **63**, 054422 (2001).

[46] S. Bausch, B. Sailer, H. Keppner, G. Willeke, E. Bucher, and G. Frommeyer, Appl. Phys. Lett. **57**, 25 (1990).

[47] I. J. Ferrer and C. Sanchez, J. Appl. Phys. **70**, 2641 (1991).

[48] G. Willeke, R. Dasbach, B. Sailer, and E. Bucher, Thin Solid Films **213**, 271 (1992).

[49] C. Hopfner, K. Ellmer, A. Enanoui, C. Pottenkofer, S. Fiechter, and H. Tributsch, J. Cryst. Growth **151**, 325 (1995).

[50] S. Ogawa, S. Waki, and T. Teranishi, Int. J. Magn. **5**, 349 (1974); S. Ogawa and T. Teranishi, Phys. Lett. **36A**, 407 (1971).

[51] Sir N. F. Mott, *Metal-Insulator Transitions*, 2nd ed. (Taylor and Francis, 1997), pp. 193.

[52] S. Ogawa, S. Waki, and T. Teranishi, Int. J. Magn. **5**, 349 (1974).

[53] H. Hiraka and Y. Endoh, J. Phys. Soc. Jpn. **63**, 4573 (1994).

[54] K. Adachi, K. Sato, M. Okimori, G. Yamauchi, H. Yasuoka, and Y. Nakamura, J. Phys. Soc. Jpn. **38**, 81 (1975).

[55] T. Takahashi, Y. Naitoh, T. Sato, T. Kamiyama, K. Yamada, H. Hiraka, Y. Endoh, M. Usada, and N. Hamada, Phys. Rev. B **63**, 094415 (2001).

[56] A. K. Mabatah, E. J. Yoffa, P. C. Eklund, M. S. Dresselhaus, and D. Adler, Phys. Rev. Lett. **39**, 494 (1977).

[57] H. S. Jarrett, W. H. Cloud, R. J. Bouchard, S. R. Butler, C. G. Frederick, and J. L. Gillson, Phys. Rev. Lett. **21**, 617 (1968).

[58] S. F. Cheng, G. T. Woods, K. Bussmann, I. I. Mazin, R. J. Soulen, E. E. Carpenter, B. N. Das, and P. Lubitz, J. Appl. Phys. **93**, 6847 (2003).

[59] R. J. Bouchard, MRS Bull. **3**, 563 (1968).

[60] G. J. Strijkers, Y. Ji, F. Y. Yang, C. L. Chien, and J. M. Byers, Phys. Rev. B **63**, 104510 (2001).

[61] G. E. Blonder, M. Tinkham, and T. M. Klapwijk, Phys. Rev. B **25**, 4515 (1982).

[62] T. J. Sato, J. W. Lynn, Y. S. Hor, and S.-W. Cheong, Phys. Rev. B **68**, 214411 (2003).

[63] K. Byczuk, M. Ulmke, and D. Volhardt, Phys. Rev. Lett. **90**, 196403 (2003).

[64] P. L. Kuhns, M. J. R. Hoch, A. P. Reyes, W. G. Moulton, L. Wang, K. Umemoto, R. M. Wentzcovitch, and C. Leighton (unpublished).

[65] Examples where the resistivity crosses over from a semiconductor-like temperature dependence to a metallic-like temperature dependence include many of the doped manganites, cobaltites, and magnetic semiconductors such as $Ga_{1-x}Mn_xAs$.

[66] A. Hamzic and I. A. Campbell, J. Phys. F: Met. Phys. **8**, L33 (1978).

[67] Two-magnon scattering processes (Refs. 65 and 66) could still be possible.

[68] T. Akimoto, Y. Moritomo, A. Nakamura, and N. Furukawa, Phys. Rev. Lett. **85**, 3914 (2000), and references within.

[69] K. Kubo and N. Ohata, J. Phys. Soc. Jpn. **33**, 21 (1972); G. Zhao, H. Keller, W. Prellier, and D. J. Kang, Phys. Rev. B **63**, 172411 (2001).

[70] S. M. Watts, S. Wirth, S. von Molnar, A. Barry, and J. M. D.

Coey, Phys. Rev. B **61**, 9621 (2000).
[71] T. R. McGuire and R. I. Potter, IEEE Trans. Magn. **11**, 1018 (1975).
[72] M. B. Salamon and M. Jaime, Rev. Mod. Phys. **73**, 583 (2001);
[73] M. Iizumi, J. W. Lynn, A. Ohsawa, and H. Ito, AIP Conf. Proc. **29**, 266 (1975).
[74] *Hand Book of Grain and Interphase Boundary Diffusion*, edited by I. Kaur, W. Gust, and L. Lozma (Ziegler, Stuttgart, 1989).
[75] L. Wang and C. Leighton (unpublished).
[76] B. Nadgorny, M. S. Osofsky, D. J. Singh, G. T. Woods, R. J. Soulen, M. K. Lee, S. D. Bu, and C. B. Eom, Appl. Phys. Lett. **82**, 427 (2003).